TRANSPORT PHENOMENA AND FLUID MECHANICS



Experimental validation of indirect conduction theory and effect of particle roughness on wall-to-particle heat transfer

Ipsita Mishra¹ | Aaron M. Lattanzi¹ | Casey Q. LaMarche¹ | Aaron B. Morris² | Christine M. Hrenya¹

Correspondence

Christine M. Hrenya, Department of Chemical and Biological Engineering, University of Colorado at Boulder, Boulder, CO 80309. Email: hrenya@colorado.edu

Abstract

Conduction between a flat wall and solid particles is important to heat transfer in various industrial unit operations. Predicting heat transfer in such systems requires theories for the two relevant modes of heat transfer: conduction through the particle-wall contact area (direct conduction), and conduction through the interstitial fluid surrounding the particles in the near-wall region (indirect conduction). While the former mechanism is well understood, experimental exploration of the latter is lacking. Here, experimental heat transfer coefficients for packed-beds of glass and steel particles are compared to computational fluid dynamics-discrete element method simulations, which include an existing theory for indirect conduction. Reasonable agreement is found when the particle Biot number (Bi) is much less than unity (steel), but significant differences occur for Bi ~ 1 (glass). Additionally, the surface morphology of the glass particles is modified to experimentally elucidate the effects of roughness on particle-wall heat transfer.

KEYWORDS

 $Biot\ number,\ DEM,\ heat\ transfer,\ indirect\ conduction,\ intraparticle\ temperature\ gradient$

1 | INTRODUCTION

Heat transfer occurring in gas-solid systems is commonplace in many industrial processes, such as the drying of wet particles in a rotary kiln, $^{1-5}$ transporting hot particulate material via pneumatic conveyors, 6,7 and processing biomass or coal in gasifiers. $^{8-10}$ In addition to conventional applications, granular material (sand) is being explored as a heat transfer fluid in concentrated solar power plants due to its cost effectiveness and ability to operate at elevated temperatures ($\gtrsim\!900^{\circ}\text{C}$) compared to traditional heat-transfer fluids. 11,12 Such widespread operations warrant a greater exploration of particulate heat transfer.

In general, the heat transfer occurring in gas-solid systems is comprised of three different mechanisms: (a) conduction, (b) convection, and (c) radiation. If the operating temperature is below 700 K, the radiation mechanism typically does not play a significant role. ^{13,14} In addition, for relatively dense and/or static systems, the interphase velocity

difference is negligible, and the contribution from convective heat transfer becomes less significant. Therefore, in dense systems at moderate temperature (T < 700K), for example, packed beds, heat exchangers, and so on, conduction is the predominant mode of heat transfer. Often times the thermal source is introduced through domain walls, and thus the heat conduction from the wall of the unit plays a crucial role in the overall heat transfer. As a result, a better understanding of particle-wall heat transfer, which is the focus of the current work, is paramount to efficient design and operation of such units. Particlewall heat transfer due to conduction is comprised of two contributions: direct conduction and indirect conduction. Direct conduction occurs across the particle-wall contact area, whereas indirect conduction occurs near the particle-wall contact through the interstitial fluid existing between the particle and the wall (i.e., particle-fluid-wall [PFW]). For stiff particles having a relatively large Young's modulus, the resulting contact area with the wall is exceedingly small; additionally, if

¹Department of Chemical and Biological Engineering, University of Colorado at Boulder, Boulder, Colorado

²School of Mechanical Engineering, Purdue University, West Lafayette, Indiana

the thermal conductivity is relatively low (e.g., glass, steel, sand, etc.), indirect conduction is expected to dominate in the system.^{15,16} Due to the significant contribution of indirect conduction to the overall heat transfer between a particle and wall for such systems, the focus of this study is further narrowed down to indirect (PFW) conduction.

Accurate prediction of the macroscopic behavior of solid particles relies heavily on the understanding of particle-level interactions (i.e., effects of particle size, surface roughness, shape, etc.), 17-20 and thus previous theoretical and numerical studies on conductive heat transfer have taken these effects into account. 15,21-23 Additionally, to understand the indirect conduction mechanism, various physical theories have been proposed, many of which incorporates the effect of microscale roughness.²⁴⁻²⁶ In particular, the Rong and Horio²⁴ theory which is being commonly used to predict heat transfer via indirect conduction is the major focus of this study. The sensitivity of the Rong and Horio²⁴ theory to particle surface roughness has been quantified using computational fluid dynamics (CFD)-discrete element method (DEM) simulations of many-particle systems. 15,16 However. no experimental validation of the theory itself, nor its dependence on surface roughness, have been reported. Rigorously testing this indirect conduction theory through experiments is a critical step in the accurate prediction of multiphase heat transfer systems in which indirect conduction plays an important role (a detailed mathematical description of this theory is presented in the next section).

To date, numerous studies have been carried out to experimentally investigate heat transfer in packed beds, 27-29 chute flows, 30-32 fluidized beds, 26,33 rotary drums, 34-38 and so on. These studies have expounded upon the effects of particle size, 30-32,39 residence time of particles, ^{29,30,36,37} and thermal conductivity of interstitial gas^{26,27,29} on heat transfer. However, the experimental endeavors to understand the effects of the microscale interactions on heat transfer is limited only to the effects of particle size, whereas the roles played by particle surface roughness and particle shape in determining macroscopic heat transfer have not been quantified. Therefore, to fill the gaps in prior experimental explorations, this work is focused on providing experimental evidence of the effects of microscale roughness on particle-wall heat transfer. Particle-scale roughness affects the particle-wall separation distance, 40-42 and thus large surface asperities (roughness) are expected to decrease the heat transfer occurring via conduction, which is consistent with previous theoretical predictions. 15,16,43-45

In this work, an experimental study is carried out to explore the link between particle surface roughness and the overall particle-wall heat transfer. The surface roughness of a set of glass particles is modified and carefully characterized, and static-bed experiments are carried out with both the modified and original particles. Furthermore, experimental results are compared with CFD-DEM predictions that incorporate the indirect conduction theory to assess the validity of the theory.²⁴ In this process, it is found that the accuracy of the indirect conduction theory, which contains an assumption of isothermal particles, depends on the particle Biot number (Bi = hR_p/k_p , where h is the heat transfer coefficient, R_p is the radius of the particle, and k_p is the thermal conductivity of the particle). The Bi represents the ratio

of the resistance to heat transfer inside a particle to the resistance to heat transfer between the particle and wall. Bi < 1 indicates that the internal resistance is less than the external fluid resistance, which has been accepted as a critical limit to assume a uniform temperature distribution inside a particle (isothermal particle). However, here it is found that the above limit is not sufficient to assume isothermal particles. Therefore, using a theoretical analysis for a single particle, the error in the prediction of heat transfer rate from the indirect conduction theory due to the isothermal particle assumption is quantified as a function of Bi. Additionally, for the purpose of robustness, experiments are also carried out with steel particles that have a smaller Bi than glass. Finally, based upon the results of this study, a critical Bi is proposed for systems dominated by indirect conduction.

2 | BACKGROUND: PARTICLE-WALL CONDUCTION THEORY

The focus of this work is on conduction through the interstitial fluid (indirect conduction or PFW conduction), while detailed accounts of conduction across the particle-wall contact area (direct conduction or particle-wall conduction) is available elsewhere. A3,46 The indirect conduction theory proposed by Rong and Horio assumes that heat transfer occurs through a static fluid surrounding the particle—the "fluid lens"—which is depicted as a dashed line in Figure 1. One-dimensional heat conduction occurs through the fluid lens when the lens overlaps with the wall. The rate of heat transfer to a single particle through the fluid lens is given by 15,16:

$$\dot{q}_{i}^{PFW} = h_{i}A_{i}\left(T_{w} - T_{p,i}\right) = H_{pfw,i}\left(T_{w} - T_{p,i}\right) = \int_{x_{in}}^{x_{out}} \frac{2\pi k_{g}x}{Max(l,s)} \left(T_{w} - T_{p,i}\right) dx \tag{1}$$

$$x_{\text{in}} = \begin{cases} x_s = \sqrt{R_p^2 - (s - R_p - \delta)^2} & \delta \le s \\ 0 & \delta > s \end{cases}$$

$$\mathbf{x}_{\text{out}} = \begin{cases} \sqrt{R_{\text{lens}}^2 - (R_{\text{p}} + \delta)^2} & \delta > \sqrt{R_{\text{lens}}^2 - R_{\text{p}}^2} - R_{\text{p}} \\ R_{\text{p}} & \delta \le \sqrt{R_{\text{lens}}^2 - R_{\text{p}}^2} - R_{\text{p}} \end{cases}$$

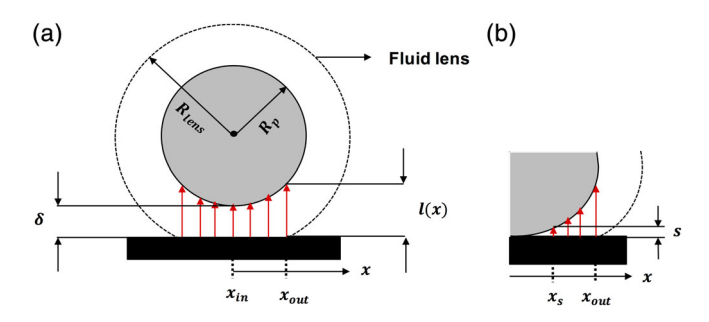


FIGURE 1 Schemata of indirect (particle-fluid-wall) conduction: (a) $\delta > s$, where δ is particle-wall separation distance and s is minimum conduction distance, and (b) $\delta < s$ [Color figure can be viewed at wileyonlinelibrary.com]

$$I(x) = (R_p + \delta) - \sqrt{{R_p}^2 - x^2}$$

where \dot{q}_i^{PFW} is the PFW heat rate for particle i, h_i is the indirect conduction heat transfer coefficient for particle i, A_i is the indirect conduction area for particle i (shown by red arrows in Figure 1), T_{w} is the wall temperature, $T_{\text{p},i}$ is the temperature of particle i, $H_{\text{pfw},i}$ is defined as the product of h_i and A_i , x is the horizontal position along the length of the wall, I(x) is the (vertical) conduction distance at a position x, s is the minimum conduction distance, δ is the particle-wall separation distance, and R_{lens} is the fluid lens radius. A complete illustration of the parameters is displayed in Figure 1.

The input parameters for the indirect conduction theory are the minimum conduction distance (s) and the fluid lens radius (R_{lens}). Physically, the minimum conduction distance s represents the asperity height for surface roughness of the particles and the wall. Mathematically, s avoids singularity in the denominator of the integral in Equation (1) at the near-wall contact. For perfectly smooth particles, s is equal to the mean free path of gas molecules, to avoid rarefaction effects. The present study is focused on particles with finite roughness, and thus the minimum conduction distance will correspond to particle surface roughness. The second input parameter-radius of the fluid lens R_{lens} —is taken to be a fraction of the particle radius, and is based upon geometric arguments. Namely, the upper bound of integration in Equation (1) (x_{out}) is limited by the radius of the particle. More specifically, one-dimensional heat conduction between a particle and wall cannot occur through the fluid lens at a radial position beyond the particle radius that is, the conduction distance (I(x)) is illdefined. Hence, from the geometrical arguments, the maximum value for the lens radius ($R_{\rm lens}$) can be found to be 1.4 $R_{\rm p}$. 11,15,16,25

3 | EXPERIMENTAL METHOD

The overarching goal of the proposed study is to quantitatively test the indirect (PFW) conduction theory described above. Thus, experiments are designed to obtain a wall-to-particle heat transfer coefficient (h) for particles in which the surface roughness is carefully characterized.

3.1 | Particle characterization

Soda lime glass particles obtained from MO-SCI Specialty Products, and AISI 52100, grade G25 steel particles, obtained from VXB ball bearings, were used in all heat transfer experiments. To reduce polydispersity, the particles were sieved into relatively narrow size ranges using standard sieves. The resulting size ranges for the glass particles are: 150–180 µm ($d_{\rm avg}$ = 165 µm), 250–300 µm ($d_{\rm avg}$ = 275 µm), and 425–500 µm ($d_{\rm avg}$ = 462 µm), and that for the steel particles is 0.85–1.18 mm ($d_{\rm avg}$ = 1 mm). The average diameter ($d_{\rm avg}$), determined as the middle of the sieve size range, is used in all the later discussions. To avoid the added effects of cohesion, the particle size ranges

below 100 μm were not considered in the experiments, and relative humidity was maintained below 20%. 47

To experimentally study the effect of roughness on heat transfer, a set of glass particles were smoothed via base etching, following a previously developed procedure. The surface topography of the particles was obtained via atomic force microscopy (AFM) measurements, as shown in Figure 2, and from the surface maps the roughness parameters, that is, root mean square roughness (rms) and peak-topeak distance (λ) were obtained. These roughness parameters can be converted into radius and height of the asperity. The asperity height is used as the minimum separation distance (λ), as given in Equation (1). The overall rms roughness is obtained for the glass particles by combining the two scales (small-scale and large-scale) of roughness, as discussed in Rabinovich et al Amarche et al Amarche et al

$$rms_{glass} = \sqrt{rms_{s,glass}^2 + rms_{L,glass}^2}$$
 (2)

where $rms_{s,glass}$ and $rms_{L,glass}$ are the small-scale and the large-scale root mean square average roughness, respectively. The root mean square roughness is then related to asperity height using a physically based constant, that is, asperity height (glass)= $1.4 \times rms_{glass}$ (eq. 6 in Rabinovich et al²⁰). The asperity height is found to be 52 nm for the smoothed (base etched) particles and 117 nm for the rough (nonetched) particles. Hence, the base etching process reduced the asperity height to approximately half of its original size. In contrast to glass, only one scale of roughness is observed in the AFM surface maps for the steel particles (nonetched). The asperity height is found to be 32 nm using the corresponding rms, that is, asperity height (steel) = $1.4 \times rms_{l steel}$.

The coefficient of sliding friction (μ) and the normal coefficient of restitution (e) for particle-particle and particle-wall were measured for both glass and steel particles, which were used as inputs to the DEM simulations described in a following section (the values are given later in Table 2). Detailed descriptions of the procedures used to measure μ and e are explained in LaMarche et al. ^{18,49} The same procedures were also followed for 1 mm steel particles. Note that for the case of glass, altering the particle roughness via base etching could affect μ , ^{50,51} and changes in frictional properties could lead to variation in e. ^{52,53} However, previous works ^{48,49} have established that the friction coefficient is not sensitive to the base etching process. Hence, the same μ and e were used for both the base etched and the nonetched particles.

The Biot number $(hR_{\rm p}/k_{\rm p})$ of the particles is found based on the indirect conduction heat transfer coefficient (h). $H_{\rm pfw}$, in Equation (1), is determined via integration over the whole indirect conduction area that is, $\pi(r_{\rm out}^2-r_{\rm in}^2)$. Hence, the h appearing in Bi refers to the areal average of $H_{\rm pfw}$:

$$h = \frac{H_{\text{pfw}}}{\pi (r_{\text{out}}^2 - r_{\text{in}}^2)}$$
 (3)

The Biot number is found to be 0.30, 0.32, and 0.35 for the 165 μ m, 275 μ m, and 462 μ m glass particles, respectively, and 0.01 for the steel particles.

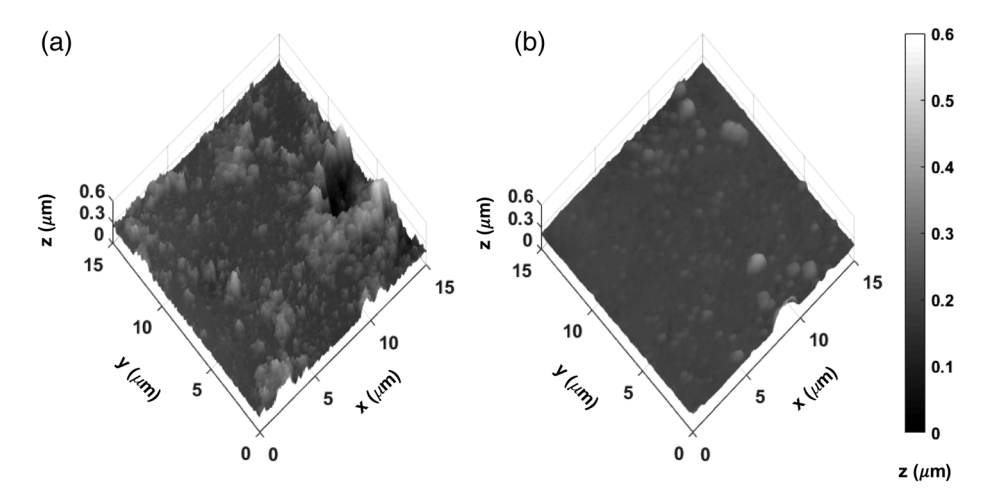


FIGURE 2 AFM surface topography maps for glass spheres: (a) rough, (b) smoothed (base-etched). AFM, atomic force microscopy

3.2 | Experimental apparatus

The experimental setup for the static bed consists of a solid aluminum block (5 cm \times 5 cm \times 8 cm) and an aluminum particle holder (5 cm \times 5 cm \times 5 cm), schematized in Figure 3. A 20 W Watlow square heating element is clamped to the bottom of the aluminum block and used to heat up the system. The whole system is placed inside a Styrofoam box to insulate the system (i.e., minimize the heat loss from the side walls). Micro-beta chip NTC thermistors (part number 100K6MCD1) are used to measure the temperature in the experiment, on account of their fast response time (~200 ms) and high accuracy (\pm 0.2°C). Shallow holes (~1.5 cm) were drilled on the aluminum blocks, where thermistors are placed. The bottom surface of the aluminum block, T_9 in the schematic given in Figure 2, is connected to a Watlow temperature controller to maintain at a constant temperature of 70° C.

The particles, initially at room temperature (~ 20° C), were dropped onto the top surface of the hot aluminum block after the block had reached steady state temperature of 70° C. As heat is transferred from the block to the particles, reading from the closest thermistor (T_1) indicates a drop in the top surface temperature of the aluminum block. One-dimensional heat conduction is assumed to occur through the block, as heat losses to the side walls have been minimized. Heat flux at the top of the aluminum block takes the form:

$$q'' = h(T_{al, surface} - T_p)$$
 (4)

where $q^{''}$ is the particle-wall heat flux, h is the heat transfer coefficient, $T_{\rm al,\ surface}$ is the temperature of the top aluminum surface, and $T_{\rm p}$ is the temperature of the particles near the wall.

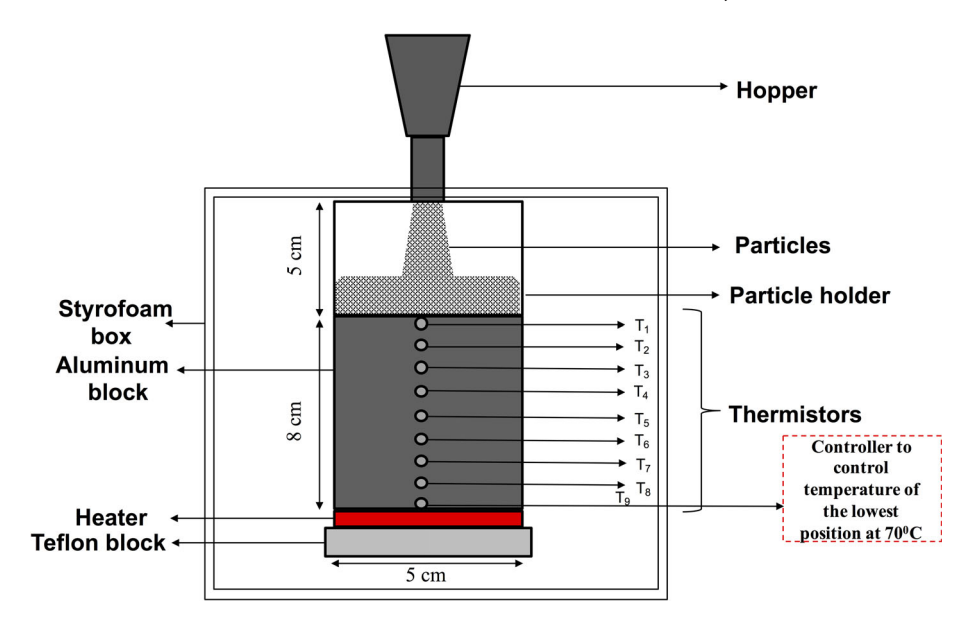
As stated above, the primary objective of the experiments is to obtain a wall-to-particle heat transfer coefficient (h) that can be used to assess the effects of particle roughness and to compare with the predictions from the indirect conduction theory.²⁴ However, to estimate h from Equation (4), the measured values of $q^{''}$, T_p , and $T_{al, \, surface}$ are required, which are difficult to measure directly from the experiment. Furthermore, $q^{''}$ varies with time, and depends on the diffusion of thermal energy to either side of the interface (i.e., to the particle bed and within the aluminum block). The introduction of room-

temperature particles on the hot aluminum surface causes a drop in the surface temperature that cannot be negated with the Watlow controller due to the time lag associated with diffusion inside the block. As per the design, the Watlow controller maintains a constant temperature at T_9 (located at the bottom of the block). However, the time associated with heat transfer through the height of the block (after particles are added to the top surface) delays the controller action to stabilize the block temperature, which is unavoidable even if temperature is controlled at T_1 (just below the top surface). Therefore, the transient heat transfer within the aluminum block and the particle bed is carefully considered to extract h from the experiment, as explained in the next section.

3.3 | Estimation of particle-wall heat transfer coefficient (h) in experiments

As previously noted, h cannot be obtained from Equation (4) in a straightforward manner as the heat flux to the particles (q") and the temperature of the particles adjacent to the wall (T_p) cannot be directly measured. Additionally, both of the above quantities (i.e., q and T_p) vary temporally. Thus, temperature measurements within the aluminum block are used in conjunction with a transient energy balance of the block to estimate h from the experiments; it is important to note that this does not involve the indirect conduction theory which we ultimately want to test the validity of. More specifically, the transient heat transfer within the aluminum block is coupled to the transient heat transfer within the packed bed via a heat flux boundary condition [Equation (4)]; the corresponding system is depicted in Figure 4. The transient energy balances for the aluminum block and the particle-bed are given by Equations (5) and (6), respectively (Table 1), where ρ_{al} is the density of aluminum, $C_{p,al}$ is the specific heat capacity of aluminum, T_{al} is the temperature of the aluminum block, $k_{\rm al}$ is the thermal conductivity of aluminum, z is the vertical position (along the height of the aluminum block or the particle-bed), ε_s is the bulk solid volume fraction of the particle-bed, $\rho_{\rm p}$ is the density of the particles, $C_{p,p}$ is the specific heat capacity of the particles, k_s is the effective thermal conductivity of the particle-bed, and T_s is the

FIGURE 3 A schematic of the experimental set up [Color figure can be viewed at wileyonlinelibrary.com]



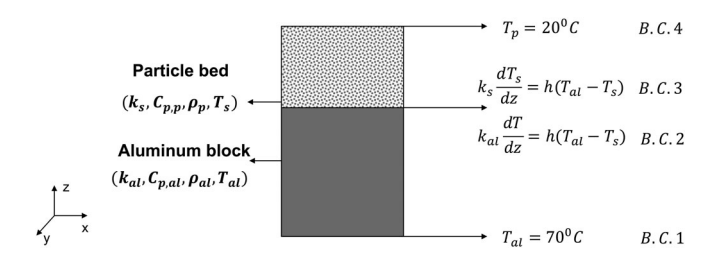


FIGURE 4 A schematic of the aluminum block and the particle-bed system

temperature of the particle-bed (all the material properties are given in Table 2). To determine the effective thermal conductivity of the particle-bed (k_s) that appears in Equation (6), the correlations given by Equations (7)–(8) in Table $1^{54,55}$ are utilized. The bulk solid volume fraction of the particle-bed (ε_s), which also appears in Equation (6), is considered 0.58, as established for the random loose packing of noncohesive particles in previous works.^{56,57} The solutions to Equations (5) and (6), in conjunction with experimental temperature measurements, are used as described below to estimate the experimental value of h.

The initial condition for the aluminum block refers to the block temperature before introducing the particles, when it is at steady state. A linear temperature profile of the aluminum block is assumed at steady state; hence, the initial temperature is determined by employing a linear interpolation between T_1 and T_9 (see Figure 3). The particle bed is initially considered at room temperature (i.e., 20° C), similar to the experiment. The boundary conditions associated with the energy equations are displayed in Figure 4: (a) the bottom of the aluminum block is maintained at a constant temperature which matches the experimental set point for T_9 , that is, 70° C, (B.C.1 in Figure 3) (b) the top of the particle bed is at a constant temperature of 20° C (B.C.4 in Figure 4), as it is exposed to the ambient conditions, and (c) the heat flux at the interface of the aluminum block and the particle bed needs to be specified (B.C.3 and B.C.4 in Figure 4). However, the interface heat flux boundary

condition involves h. To estimate h, the Nusselt correlation proposed by Morris et al¹⁵ for indirect conduction in a multiparticle system [Equations (9)-(11) in Table 1] is used. In the Nusselt correlation, for a specific interstitial fluid and particle size, the particle diameter (d_n) , gas conductivity (k_g), and Nu_{max} are known constants. Therefore, h is only a function of the near-wall solid volume fraction ($\varepsilon_{\text{s,wall}}$). Because direct measurement of $\varepsilon_{\mathrm{s,wall}}$ is difficult for each experimental run, a trial-anderror method is adopted. In this method, an initial guess for $\varepsilon_{s,-}$ $_{\text{wall}}$ is taken from a previously reported range of 0.55–0.58 56,57,59 and used in the solution of the equations in Table 1. Subsequent guesses for $\varepsilon_{s,wall}$ are tried until the temperature profile obtained from the transient solutions (which were solved numerically using the finite difference method) match the experimentally observed trend, and the drop at T_1 matches the experimental value, as depicted in Figure 5a. Using this final value of $\varepsilon_{\rm s,wall}$, the experimental value of h can then be estimated from Equations (9)-(11).

The temperature profile for the particle bed obtained from the transient solutions after 1 s, as shown in Figure 5b, suggests that heat penetration inside the bed is negligible over the considered time scales, which is physically consistent with the aim of this work that is, quantifying the interfacial wall-to-particle heat transfer rather than the bulk solids heat transfer. Furthermore, a statistically significant temperature drop at T_1 , as evidenced by the nonoverlapping error bars in Figure 5a, indicates that the role of the experimental uncertainties after 1 s is negligible in the described method. Thus, by solving the transient energy equations with the help of the trial-and-error method, an experimental heat transfer coefficient is extracted.

3.4 | CFD-DEM simulations

The objective of the CFD-DEM simulations is to predict the wall-toparticle heat transfer coefficient for the many-particle system based upon Rong and Horio's theory for indirect conduction. Predictions are then compared with those extracted from the experiments to assess

TABLE 1 Summary of equations to estimate particle-wall heat transfer coefficient

Aluminum block: energy balance	$ \rho_{al} C_{p,al} \frac{\partial T_{al}}{\partial t} = k_{al} \frac{\partial^2 T_{al}}{\partial z^2} $		5
Particle bed: energy balance	$\varepsilon_{s}\rho_{p}C_{p,p}\frac{\partial T_{s}}{\partial t} = \varepsilon_{s}k_{s}\frac{\partial^{2}T_{s}}{\partial z^{2}}$		6
Correlation for the effective conductivity of particle bed ^{54, 55, 58}	$\frac{k_s}{k_g} = \frac{\phi_k \left(\frac{k_p}{k_g}\right) + (1 - \phi_k)\lambda_r}{\sqrt{\varepsilon_s}}$ $\phi_k = 7.26*10^{-3}$		7
	$\lambda_{r} = \frac{-2}{1 - b_{kp}^{kg}} \left[\frac{\binom{\frac{k_{p}}{k_{g}} - 1}{b_{kp}^{kg}}}{\binom{1 - b_{kp}^{kg}}{b_{p}^{kg}}} \ln \left(b \frac{k_{g}}{k_{p}} \right) + \frac{b - 1}{1 - b_{kp}^{kg}} + \frac{b + 1}{2} \right]$ $b = 1.25 \left(\frac{1 - e_{g}}{\epsilon_{g}} \right)^{10/9}$		8
Nusselt correlation ¹⁵	$\frac{Nu}{Nu_{max}} = C_0 + C_1 \varepsilon_{s,wall} + C_2 \varepsilon_{s,wall}^2 + C_3 \varepsilon_{s,wall}^3 + C_4 \varepsilon_{s,wall}^2$	$_{\text{s,wall}}^{4} + C_{5}\varepsilon_{\text{s,wall}}^{5} + C_{6}\varepsilon_{\text{s,wall}}^{6} + C_{7}\varepsilon_{\text{s,wall}}^{7}$	9
	$C_0 = 1.0838 \times 10^{-3}$ $C_2 = 2.4268 \times 10^0$ $C_4 = -1.2243 \times 10^2$ $C_6 = -1.1706 \times 10^3$	$C_1 = -2.1709 \times 10^{-2}$ $C_3 = 1.9101 \times 10^0$ $C_5 = 6.1504 \times 10^2$ $C_7 = 7.9093 \times 10^2$	
	$Nu = \frac{hd_p}{k_g}$		10
	$Nu_{\text{max}} = \frac{1}{2}\hat{H}(0)$		11
	$\begin{split} \hat{H}(0) &= \int_{\hat{r}_{in}}^{\hat{r}_{out}} \frac{2\pi \hat{r}}{\sqrt{1-\hat{r}^2}-1} d\hat{r} \left(\hat{r} = \frac{r}{R_p}\right) \\ \hat{r}_{in} &= \sqrt{1 - \left(1 - \frac{s}{R_p}\right)^2} \\ \hat{r}_{out} &= 1 \end{split}$		

TABLE 2 Material properties

Parameters	Glass	Steel	Aluminum
Diameter, d_{avg} (m)	165, 275, 462	1,000	
Density, ρ (kg/m ³)	2,500	7,810	2,700
Thermal conductivity, k (W/m K)	1.1	46.6	167
Specific heat capacity, C _p (J/kg K)	795	502	896
Young's modulus, E (G Pa)	72	200	69
Poisson's ratio, ν (dimensionless)	0.17	0.28	0.33
Coefficient of friction (particle- particle)	0.275	0.211	
Coefficient of friction (particlewall)	0.334	0.209	
Normal coefficient of restitution (particle-particle)	0.97	0.94	
Normal coefficient of restitution (particle-wall)	0.86	0.68	

the accuracy of the theory, with particular emphasis placed on the effect of surface roughness.

The geometry for the simulation consists of a 5 cm \times 5 cm \times 5 cm cube, which is the same size as the particle holder in the experiment. Initially, particles are placed at randomly generated positions without overlap in a domain of 2 cm \times 2 cm \times 4 cm (length \times width \times height), as shown in Figure 6a. The initialization of the particles was analogous to the experimental configuration, where particles fall from a hopper placed just above the particle holder (see Figure 3). The particles fall under the

force of gravity, and bouncing continues for a short time before the system becomes static, as shown in Figure 6b. As the focus is only on wallto-particle heat transfer, the number of particles in the simulation was limited to a value that can form roughly two to three layers on the bottom wall, instead of filling up the whole container, which greatly reduces the computational cost (The maximum computational time was 118 days for 165 µm particles, using 42 Intel(R) Xeon(R) 2.40GHz processors in parallel). Any additional layer of particles added to the top of the bed may slightly change the temperature profile of the particles within the bed and thus also the heat flux (q'') into the system (as q'' is proportional to the temperature difference between wall and particles). However, the quantity of interest here—the heat transfer coefficient (ratio of heat flux to the temperature difference between the wall and particles)-will remain the same. Furthermore, the load from added layers of particle can affect the particle-wall overlap, and thus also the heat transfer coefficient (h) [by changing δ in Equation (1)]. However, calculations to estimate this change in overlap indicate that due to high Young's modulus of the particles considered here, the effect of load on h is negligible for the systems considered here. Therefore, increasing the number of layers will not effectively change the resulting wall-to-particle heat transfer coefficient. The other means by which the computational time could be reduced is via a narrower domain with periodic side walls. However, as the emphasis here is on replicating the exact experimental set up without changing any possible wall effects, this method was not adopted. The bulk solid volume fraction of the particles in the simulation lies between 0.57 and 0.58.

The CFD-DEM simulations were carried out using MFIX, an open source code developed by U.S. DOE National Energy Technology

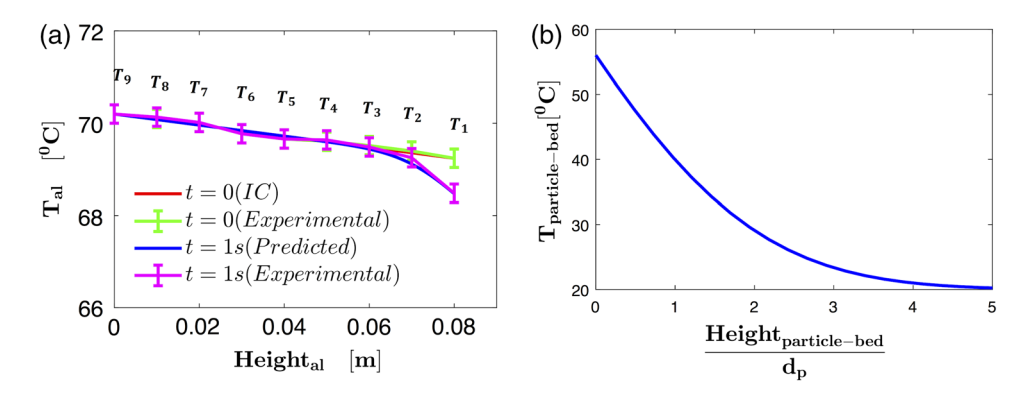


FIGURE 5 (a) Demonstration of estimating in experiments for which the experimental temperature profile (magenta line) coincides with that from the transient solution after 1 s for the aluminum block (blue line). Error bars represent accuracy of the thermistor, that is, $\pm 0.2^{\circ}$ C. (b) Temperature variation inside the particle-bed for 165 μ m obtained from the transient solutions after 1 s [Color figure can be viewed at wileyonlinelibrary.com]

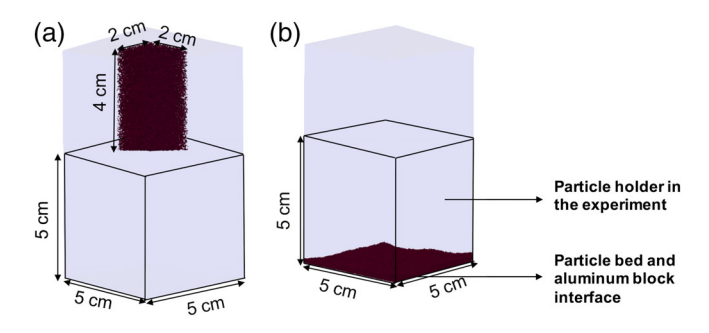


FIGURE 6 System used in the simulation (a) initialization of the particles, (b) static bed (after bouncing of the particles is completely stopped) [Color figure can be viewed at wileyonlinelibrary.com]

Laboratory (NETL),⁶⁰ to obtain the heat transfer coefficient for a static bed of particles. The particles are considered monodisperse in the simulation, using the arithmetic mean of each sieved size range for the particle diameter. The CFD solver is implemented for the (continuum) fluid phase and the DEM is used to track the position and velocities of discrete particles. The governing momentum and energy balances implemented in CFD and DEM are the same as those presented in Morris et al¹⁵ and Lattanzi and Hrenya.⁶¹

In the simulations, a free slip boundary condition for the fluid phase was imposed on all side walls and the bottom wall, whereas the top boundary was given a constant pressure (ambient) boundary condition. The energy equations for both the fluid and the solid phase were solved by implementing boundary conditions similar to the experiment, that is, all the side walls of the particle bed are adiabatic, and the top boundary temperature is equal to the ambient temperature (20°C). However, the bottom boundary condition differs from the experiment. Namely, a constant temperature of 70°C was specified on the bottom wall in the simulation rather than a time varying heat flux; the reason and implications of this difference are addressed below. Implementation of all the above boundary conditions in multiphase systems is well documented.⁶²

Note that the bottom wall in the simulation refers to the interface between the particle bed and aluminum block in the experiment (see Figure 6b). The top surface temperature of the aluminum block will drop in the experiment due to heat transfer with the particles once they are dropped, and thus the heat transfer to the particles is inherently coupled to the heat transfer within the aluminum block. Because direct measurement of the particle temperature near the wall and the interface heat flux is not straightforward, Equation (4) cannot be used to calculate h directly. Instead, h is extracted from the measured value of the aluminum surface temperature drop just after particles are dropped, as described above. In contrast, DEM simulations provide the values for the wall-to-particle heat flux and the temperatures of the particles as a function of time, allowing h to be calculated directly from Equation (4).

Due to the difference in the boundary condition between experiments and DEM simulations, the temperature gradient between the wall and particles (ΔT) in the simulation may differ slightly from that of the experiments. Recall that the heat transfer coefficient is the constant of proportionality between heat flux (q'') and temperature gradient (ΔT), that is, $h = \frac{q \nu}{\Delta T}$; hence, h will remain constant with changes in ΔT as $q^{\prime\prime}$ will change proportionally. Furthermore, the heat transfer coefficient for indirect conduction, which is the dominant mode of heat transfer, is a function of particle size (Rp), particle-wall proximity (δ), and the thermal conductivity of the interstitial fluid (k_g), as given in Equation (1). The thermal conductivity of air (k_g) is not a strong function of temperature and thus the heat transfer coefficient is effectively independent of temperature. Additionally, the particle-wall separation distance (δ) stays fixed for a static system. Therefore, the small difference in ΔT between the experiments and simulation will not alter the resulting heat transfer coefficient.

The material properties and the simulation parameters needed to solve the momentum and energy balances are outlined in Tables 2–4. For the input parameters [i.e., s and $R_{\rm lens}$ in Equation (1)], the measured values of particle surface roughness and the maximum value for $R_{\rm lens}$ from the geometrical arguments [i.e., $R_{\rm lens}$ = $1.4R_{\rm p}$ in Equation (1)]^{15,16} were used. In addition to the above physical inputs, a numerical input, that is, the time step for temporal averaging of the parameters obtained at each solid time step ($t_{\rm avg}$ in Table 3), was specified. Here, $t_{\rm avg}$ is equal to the time interval considered in the experimental data acquisition. The wall-to-particle heat transfer rate prediction in DEM ($\dot{q}_{\rm total}$) accounts for contributions from both the PFW and particle-wall heat

transfer (indirect and direct conduction, respectively). However, the contribution from the PFW heat transfer is up to three orders of magnitude higher than the particle-wall heat transfer for the particles considered here and thus indirect conduction is effectively isolated. To extract the heat transfer coefficient predicted by DEM simulations, both the wall-to-particle heat rate and temperature of the particles are averaged temporally over t_{avg} . The heat transfer coefficient for the bottom plate is then calculated by dividing the total heat rate (\dot{q}_{total}) by the surface area of the bottom wall (i.e., $A_{wall} = 25 \text{ cm}^2$) and the temperature difference between wall and particles, $h_{\text{DEM}} = \frac{\dot{q}_{total}}{A_{wall}(T_w - T_{p,avg})}$.

4 | RESULTS AND DISCUSSION

4.1 | Experiments: effect of particle size and surface roughness on heat transfer

The experimental heat transfer coefficient for the three different sizes (i.e., 165, 275, and 462 μ m) of rough glass particles are obtained as described previously. The heat transfer coefficient is observed to increase with a decrease in particle size, as shown in Figure 7a. The above trend for particle size has been widely observed in various

TABLE 3 Simulation parameters

Spring constant, k_n (N/m)	10 ³
CFD cell size (m)	0.001
Fluid time step (s)	10^{-4}
Solid time step (s)	10^{-7}
Time step for temporal averaging, $t_{\rm avg}$ (s)	10-3

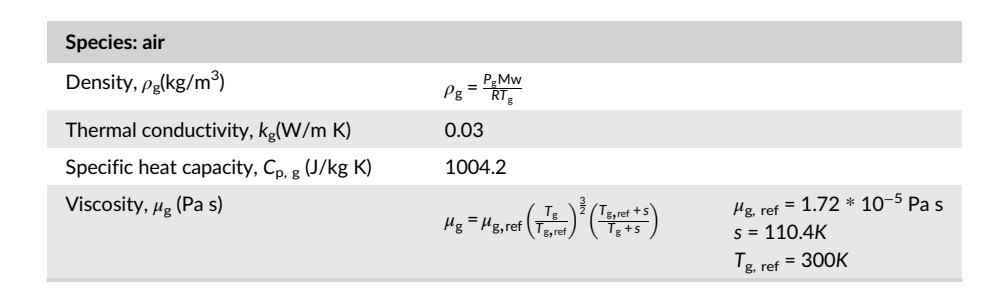
Abbreviation: CFD, computational fluid dynamics.

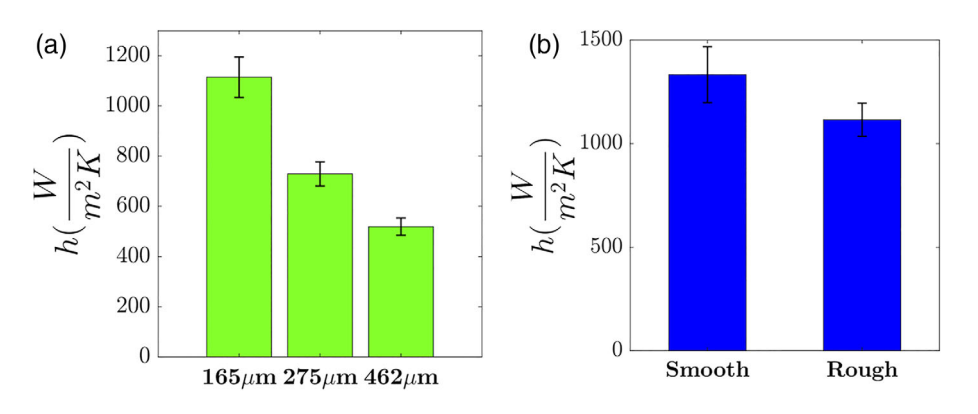
previous experimental works. $^{30\text{-}32,39,63}$ The corresponding near-wall solid volume fractions for the three different size ranges utilized to extract h from the experiments are 0.53 ± 0.02 , 0.53 ± 0.01 , and 0.54 ± 0.01 , respectively. The range on each of the solid volume fractions was determined based upon a 95% confidence interval. The assumed solid volume fractions are close to the previously reported values in the near wall regime for the random loose packings, that is, 0.55-0.58. 56,57,64,65

Next, the effect of surface roughness on particle-wall heat transfer is established. The results, shown in Figure 7b, suggest that smooth particles have a higher h value than their rough counterparts, which is in qualitative agreement with the predictions of indirect conduction theory. The solid volume fraction estimated from the experiments for the smooth 165 μ m particle set is 0.54 \pm 0.01. The nonoverlapping confidence intervals, shown in Figure 7b, indicate a small, but statistically significant difference between the smooth- and rough-particle heat transfer. The simulation study carried out for a single particle in Morris et al suggests that with the same surface roughness, the effect of roughness on heat transfer is more prominent for a smaller diameter particle. Hence, experiments were carried out only for the smallest size (165 μ m) to observe the maximum effect due to a change in surface roughness.

The percentage change in the heat transfer coefficient due to a decrease in the asperity height (surface roughness) to half of the original value is around $16\pm8\%$ for the $165~\mu m$ particles. Therefore, the experiments reveal that in addition to particle size, surface roughness will also alter the heat transfer coefficient, but the percentage change is small for the current level of change in roughness. The comparison between the experimental results and the CFD-DEM predicted results, for the same system and the same change in the asperity height, is discussed in the following section.

TABLE 4 Gas properties





right rough (a) Heat transfer coefficient for three different sizes of rough (nonetched) glass particles and (b) heat transfer coefficient for rough and smooth (etched) glass particles of the size 165 µm. Error bars represent 95% confidence interval, based on 20 trials each [Color figure can be viewed at wileyonlinelibrary.com]

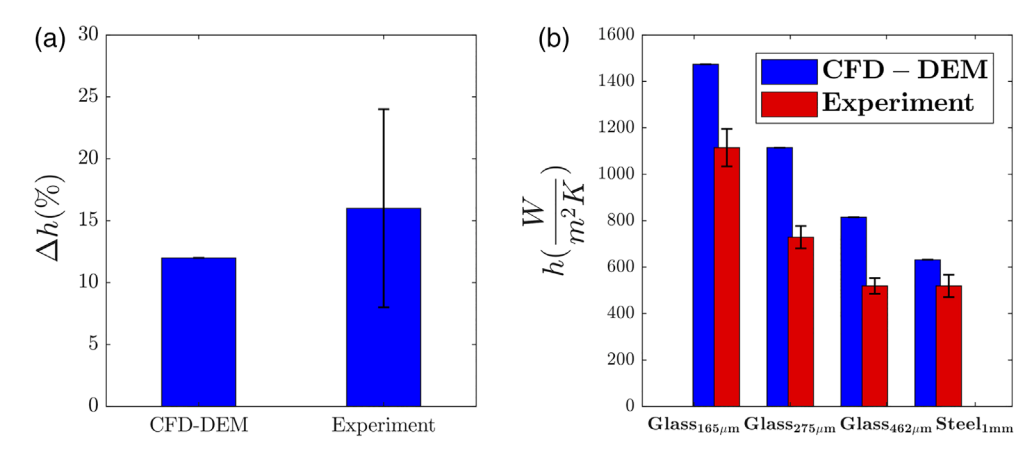


FIGURE 8 Comparison between experiments and CFD-DEM simulations: (a) percentage change in heat transfer coefficient (between the smooth and the rough particle set of $165 \mu m$) (error bars are based upon experimental error propagation) and (b) heat transfer coefficient (h) for glass as well as for steel particles (error bars represent 95% confidence interval). CFD, computational fluid dynamics; DEM, discrete element method [Color figure can be viewed at wileyonlinelibrary.com]

4.2 | Experiment versus theory: assessment of validity of indirect conduction theory

4.2.1 | Comparison between experiments and CFD-DEM simulations for glass

The heat transfer coefficient (h) is determined from the CFD-DEM simulations, which include the indirect conduction theory [Equation (1)],²⁴ for the three different sizes of glass particles (165, 275, and 462 μm) and 1 mm steel particles. The percentage change in h (Δh) due to the change in surface roughness for 165 µm glass particles is in agreement between the experiments and simulations, shown in Figure 8a. However, the actual value of the heat transfer coefficient for all the glass particles are over-predicted by the CFD-DEM simulations, as depicted in Figure 8b. Furthermore, a Gaussian distribution of particles encompassing the experimentally sieved size range was used in the simulations to explore the effect of polydispersity on the predicted heat transfer coefficient (h). The results show a less than 1% change in h indicating polydispersity does not play a significant role. The predictions for steel are markedly closer to their experimental counterparts. Our hypothesis on the cause of the discrepancy for the glass particles is detailed in the next section.

4.2.2 | Reason for the discrepancy between experiment and CFD-DEM simulation results

We hypothesize that if intraparticle temperature gradients are significant, the experimental heat transfer coefficient (h) will be lower than the CFD-DEM predictions which assumes isothermal particles. More specifically, if the internal resistance is high (i.e., low thermal conductivity), then temperature gradients within the particle will be significant. Recall that the local heat transfer coefficient for indirect conduction is inversely proportional to the wall-to-particle perpendicular distance (I(x)), as evident from Equation (1). Accordingly, in the

near wall region where l(x) is the minimum, the local heat transfer coefficient will be very large, and the particle surface temperature is expected to deviate from the temperature at the particle center. This high surface temperature leads to a smaller driving force for heat transfer relative to the isothermal counterpart (high thermal conductivity), thereby resulting in a lower heat flux (i.e., lower drop in aluminum surface temperature when particles are released). As described in the previous section, the experimental heat transfer coefficient (h) is extracted via matching the temperature drop of the aluminum surface. Hence, a lower value of h is expected when the particles are nonisothermal.

To study the temperature distribution inside a glass particle, the transient energy equation within a sphere,

$$\rho C_{p} \frac{\partial T}{\partial t} = \frac{1}{r^{2}} \frac{\partial}{\partial r} \left(r^{2} k \frac{\partial T}{\partial r} \right) + \frac{1}{r^{2} \sin^{2} \theta} \frac{\partial}{\partial \theta} \left(k \frac{\partial T}{\partial \theta} \right) + \frac{\partial}{\partial \theta} \left(\sin \theta \dot{K} \frac{\partial}{\partial \theta} \left(\sin \theta \dot{K} \frac{\partial T}{\partial \theta} \right),$$
(12)

was solved using PDE toolbox in MATLAB,66 which employs the finite element method. As the focus here is to determine the temperature variation within a particle due to indirect conduction, the heat flux boundary condition on the bottom half of the particle surface is given by Equation (1) and an adiabatic boundary condition is used on the top half, for the sake of simplicity. A 500 μm diameter particle (the largest size glass particle used in the experiment), with a Biot number (Bi) of 0.35, is considered here. The particle-wall separation distance (δ) is set equal to the minimum separation distance (i.e., s = 117 nm), and the wall temperature (T_w) is given a value of 70° C. Initially, the particle is assumed to be at room temperature (20°C). The same procedure was followed for a steel particle of the same size, which is characterized by Bi = 0.01. The system time (t) is nondimensionalized using the particle properties, that is, density (ρ) , heat capacity (C_p) , particle volume (v), and the areal heat transfer coefficient (H_{pfw}); the characteristic, nondimensional time (t^*) can be expressed as $t^* = \frac{n_{pfw}t}{\rho C_p v^*}$

Temperature profiles for each particle are obtained at different time steps, as shown in Figure 9a,b, respectively. The results suggest that significant temperature gradients exist within the glass particle, as is most prominent at the characteristic time $t^*=1$, whereas the temperature distribution within the steel particle remains relatively uniform at all times. For the glass particle, temperature varies in both the horizontal (x) and vertical (z) direction, as shown in Figure 9a. Correspondingly, the particle-wall temperature gradient ($T_w - T_p$) is a function of x, as well as of z; the modified Equation (1) is given by:

$$\dot{q}_{i}^{\text{PFW}}(t) = H_{\text{pfw},i} \left(T_{\text{w}} - T_{\text{p},i}(t) \right) = \int_{x_{\text{in}}}^{x_{\text{out}}} \int_{z=0}^{z=R_{\text{p}}} \frac{2\pi k_{\text{g}} x}{\text{Max}(\textit{I},s)} \left(T_{\text{w}} - T_{\text{p},i}(x,z,t) \right) dx dz \ . \tag{13}$$

A comparison of isothermal [Equation (1)] and nonisothermal [Equation (13)] wall-to-particle heat rates is shown for glass and steel in Figure 10a,b, respectively. It is evident from the plot that the isothermal assumption in indirect conduction theory over-predicts the heat rate significantly for the glass particle, but not for steel. Therefore, the heat transfer coefficient predictions from CFD-DEM with the indirect conduction theory²⁴ (assumes isothermal particle) are expected to be in better agreement with the experiments for the steel particles as compared to glass.

4.2.3 | Comparison between experiment and CFD-DEM simulation for steel

As stated above, close agreement between experimental and DEM predictions for h is observed for steel particles relative to that of glass, shown in Figure 8b. Thus, in the absence of prominent intraparticle temperature gradients, more accurate predictions can be made from indirect conduction theory. Moreover, the corresponding near-wall solid volume fraction ($\varepsilon_{s,wall}$) for the steel particles, used to estimate the experimental h, is 0.58 \pm 0.007, which lies within the previously

reported $\varepsilon_{\rm s,wall}$ range that is, 0.55–0.58.^{56,57,64,65} The estimated $\varepsilon_{\rm s,wall}$ for glass particles (0.53 ± 0.02, 0.53 ± 0.01, and 0.54 ± 0.01) are slightly less than that for steel. One possible explanation for the above trend may be the nonisothermal behavior of the former compared to the latter. As explained in a previous section, intraparticle temperature gradients decrease h. Hence, in Equation (9), which inherently assumes isothermal particles, a lower $\varepsilon_{\rm s,wall}$ is used to obtain the correct h.

Note that there is still a small discrepancy (i.e., ~17%) between the experimental and simulation results for steel, which may be attributed to various other factors that could affect the particle-wall heat transfer. For example, variations in thermal conductivity of the fluid (k_p) due to slight changes in relative humidity, uncertainties in surface roughness measurement, solid volume fraction near the wall, and so on, may impact the heat transfer coefficient. The sensitivity studies carried out via CFD-DEM simulations show that a 10-20% change in relative humidity results in ~3% change in the heat transfer coefficient (h). Similarly, ~5% change in h is predicted by changing the minimum conduction distance parameter by 5 nm, which is the observed SD for the measured values of roughness. Furthermore, the changes in the near wall solid volume fraction within the error bars presented above (i.e., 0.007) have a more significant impact (~12%, using the correlation given by Morris et al¹⁵), which can bring the simulation results within the experimental error bar (results not presented for the sake of brevity).

4.3 | Biot number

Due to the discrepancy in predictions observed for the glass particles and traced to nonisothermal effects, a closer examination of the Biot number (Bi) is warranted. In previous works with sand particles, the transport of thermal energy within the particles has been assumed relatively uniform when Bi < 1.^{15,29,30,39,67} However, in the present study, the intraparticle temperature gradients in glass lead to a mismatch between theory and experiments. The maximum Bi for glass

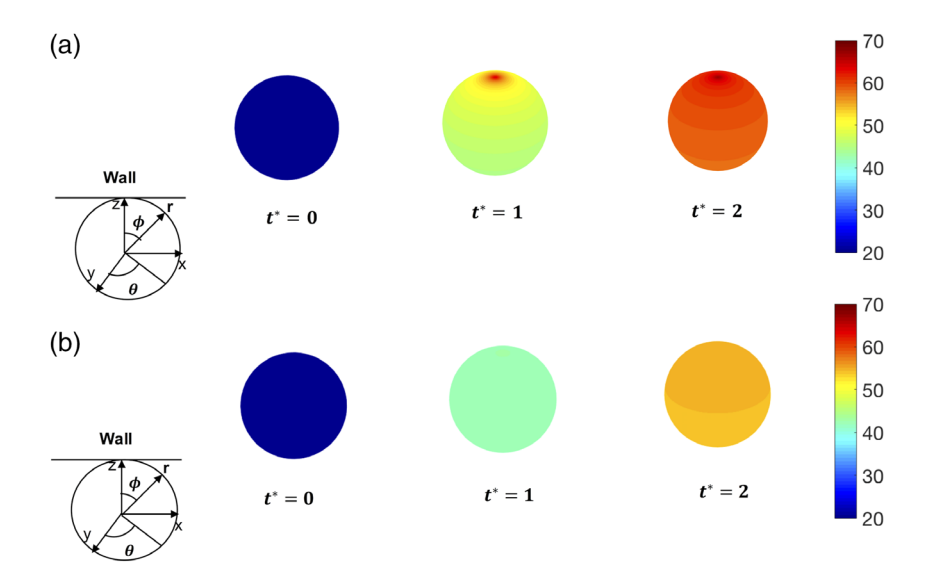


FIGURE 9 Internal temperature profiles for the particles obtained from solving the energy equation in spherical coordinates for (a) glass and (b) steel. In the above figures, the hot wall is near the top of the particle, instead of bottom, to clearly show the intra particle temperature gradients [Color figure can be viewed at wileyonlinelibrary.com]

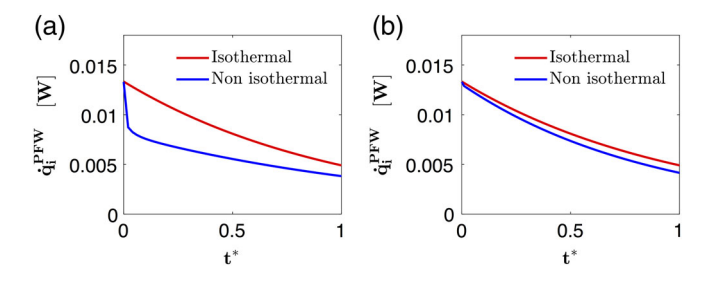


FIGURE 10 Heat rate profiles determined under isothermal and nonisothermal conditions for (a) 500 μm glass, (b) 500 μm steel particle [Color figure can be viewed at wileyonlinelibrary.com]

particles used in the experiments is 0.35, which is below the previously asserted critical limit (Bi < 1). Therefore, the impacts of intraparticle temperature gradients in predicting the heat transfer rate from the indirect conduction theory²⁴ are rigorously characterized below.

The error in the predicted heat rate was evaluated by carrying out finite element simulations for a single particle in MATLAB, as previously explained. The finite element simulations capture the spatially varying temperature distribution inside the particle and allow the heat rate to a nonisothermal particle $(\dot{q}_{i,\text{nonisothermal}}^{\text{PFW}})$ to be calculated via Equation (13), while the isothermal heat rate $(\dot{q}_{i,\text{isothermal}}^{\text{PFW}})$ can be determined from Equation (1). As the error between $\dot{q}_{i,\text{nonisothermal}}^{\text{PFW}}$ and $\dot{q}_{i,\text{isothermal}}^{\text{PFW}}$ will vary in time, a time averaged percent error $(E_{\text{nonisothermal}})$ is determined:

$$E_{\text{nonisothermal}}(\%) = \frac{1}{\tau} \int_{0}^{\tau} \frac{\dot{q}_{i,\text{isothermal}}^{\text{PFW}} - \dot{q}_{i,\text{nonisothermal}}^{\text{PFW}}}{\dot{q}_{i,\text{isothermal}}^{\text{PFW}}} dt \times 100 \tag{14}$$

where $\dot{q}_{i,\, \text{isothermal}}^{\text{PFW}}$ and $\dot{q}_{i,\, \text{nonisothermal}}^{\text{PFW}}$ are determined from Equations (1) and (13), respectively; $\tau = \frac{\rho C_{p} v}{h_{p f w}}$ defines a characteristic time for a system that is evaluated based upon particle properties (i.e., ρ , C_p , v) and the heat transfer mechanism predominant in the system (e.g., indirect conduction in the present study). As shown in Figure 9a, intraparticle temperature variation will be most prominent for $t \le \tau$ (or $t^* \le 1$) when the particle is undergoing most of its heating (i.e., the particle is far from thermal equilibrium with the wall); therefore, the temporal averaging is carried out over τ .

As depicted in Figure 11, the percentage error will be less than 10% for Bi < 0.015, which is the critical Bi proposed here for systems dominated by indirect conduction. Nonetheless, the indirect conduction theory can be applied for a wider range of Bi if a lower accuracy is permissible, based on the relation depicted in Figure 11. Furthermore, the percentage error between the experimental and theoretical heat transfer coefficient (from Figure 8b) is presented in Figure 11. The error above can be attributed to a wide variety of factors: variations in relative humidity, roughness measurement, solid volume fraction, and so on, in addition to the intraparticle temperature gradients. However, the overlapping error bars in Figure 11 indicate that the intraparticle temperature gradients are the major contributor for the discrepancy.

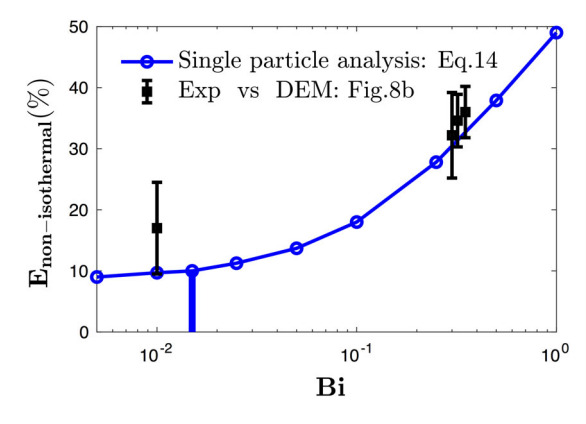


FIGURE 11 Percentage error in the heat rate prediction due to the isothermal particle assumption for different, from a theoretical analysis [Equation (14)] and from comparison between experiments and DEM simulations, given in Figure 8b. Error bars are based upon the experimental error propagation. DEM, discrete element method [Color figure can be viewed at wileyonlinelibrary.com]

5 | CONCLUDING REMARKS

Numerous studies have been carried out to show the role of particle-scale properties on the hydrodynamic behavior of granular materials, such as fluidization, 18 clustering, 19 bulk stress, 68 and so on. However, for granular heat transfer, the role of particle-scale properties has not been well vetted experimentally. A systematic experimental study is carried out here by isolating the surface roughness to establish the sensitivity of particulate heat transfer, and particularly indirect conduction, to this microscale property. Furthermore, to assess the validity of the indirect conduction theory proposed by Rong and Horio, ²⁴ where particle surface roughness is a theoretical input, experimental results are compared with CFD-DEM predictions that implement this theory. Excellent agreement is observed for the qualitative trends in the heat transfer coefficient (h) due to a change in surface roughness. However, it is found that the quantitative agreement between DEM and experimental results is influenced by the particle Biot number (Bi). The discrepancy observed for glass particles (higher Bi) is traced to the nonuniform temperature distribution inside the particles. Based on the error in the heat transfer rate due to the isothermal assumption (obtained from a theoretical analysis), a critical Bi is proposed for systems governed by indirect conduction.

Overall, the experiments carried out in the current work have established the effects of surface roughness. To establish a better understanding of the role played by particle scale properties, a next logical step is the evaluation of particle-shape effects. Moreover, the results suggest that depending upon the particle Biot number, a certain percentage of over-prediction in h is expected from the indirect conduction theory due to its inherence assumption of an isothermal particle. Recently, Oschmann et al⁶⁹ have proposed a DEM model to resolve the heat transfer inside a particle, which is appropriate for systems above the critical Bi established here.

ACKNOWLEDGMENTS

The authors gratefully acknowledge the National Science Foundation for providing funding for this work via grant. The authors also thank Ben Grote for his help with portions of the experimental work.

ORCID

Ipsita Mishra https://orcid.org/0000-0002-2486-137X *Casey Q. LaMarche* https://orcid.org/0000-0002-6197-5747

REFERENCES

- Shi D, Vargas WL, McCarthy JJ. Heat transfer in rotary kilns with interstitial gases. Chem Eng Sci. 2008;63(18):4506-4516. https://doi. org/10.1016/j.ces.2008.06.006.
- Figueroa I, Vargas WL, McCarthy JJ. Mixing and heat conduction in rotating tumblers. Chem Eng Sci. 2010;65(2):1045-1054. https://doi. org/10.1016/j.ces.2009.09.058.
- Spurling RJ, Davidson JF, Scott DM. The no-flow problem for granular material in rotating kilns and dish granulators. *Chem Eng Sci.* 2000;55 (12):2303-2313. https://doi.org/10.1016/s0009-2509(99)00528-x.
- Yohannes B, Emady H, Anderson K, et al. Scaling of heat transfer and temperature distribution in granular flows in rotating drums. *Phys Rev* E. 2016;94(4):156. https://doi.org/10.1103/PhysRevE.94.042902.
- Emady HN, Anderson KV, Borghard WG, Muzzio FJ, Glasser BJ, Cuitino A. Prediction of conductive heating time scales of particles in a rotary drum. *Chem Eng Sci.* 2016;152:45-54. https://doi.org/10. 1016/j.ces.2016.05.022.
- Li J, Mason DJ. A computational investigation of transient heat transfer in pneumatic transport of granular particles. *Powder Technol.* 2000; 112(3):273-282. https://doi.org/10.1016/S0032-5910(00)00302-8.
- Bandrowski J, Kaczmarzyk G. Gas-to-particle heat transfer in vertical pneumatic conveying of granular materials. *Chem Eng Sci.* 1978;33 (10):1303-1310. https://doi.org/10.1016/0009-2509(78)85111-2.
- Zhou ZY, Yu AB, Zulli P. A new computational method for studying heat transfer in fluid bed reactors. *Powder Technol.* 2010;197(1-2): 102-110. https://doi.org/10.1016/j.powtec.2009.09.002.
- de Souza-Santos ML. Solid Fuels Combustion and Gasification: Modeling, Simulation. Boca Raton: CRC Press; 2010.
- Corella J, Toledo JM, Molina G. A review on dual fluidized-bed biomass gasifiers. *Ind Eng Chem Res.* 2007;46(21):6831-6839. https://doi.org/10.1021/ie0705507.
- Morris AB, Ma Z, Pannala S, Hrenya CM. Simulations of heat transfer to solid particles flowing through an array of heated tubes. *Solar Energy*. 2016;130(C):101-115. https://doi.org/10.1016/j.solener. 2016.01.033.
- Martinek J, Ma Z. Granular flow and heat-transfer study in a nearblackbody enclosed particle receiver. J Sol Energy Eng. 2015;137(5): 051008. https://doi.org/10.1115/1.4030970.
- Flamant G, Menigault T. Combined wall-to-fluidized bed heat transfer. Bubbles and emulsion contributions at high temperature. *Int J Heat Mass Transf.* 1987;30(9):1803-1812. https://doi.org/10.1016/0017-9310(87)90239-0.
- Wen CY, Chang TM. Particle to particle heat transfer in air fluidized beds. Proceedings of International Symposium on Fluidization; June 6–9; Eindhoven, Netherlands, 1967. https://doi.org/10.1002/aic. 12049/full
- Morris AB, Pannala S, Ma Z, Hrenya CM. A conductive heat transfer model for particle flows over immersed surfaces. *Int J Heat Mass Transf*. 2015;89(C):1277-1289. https://doi.org/10.1016/j.ijheatmasstransfer. 2015.06.004.

- Lattanzi AM, Hrenya CM. Indirect conduction in gas-solids systems: static vs. dynamic effects. AIChE J. 2017;30(9):1803-4693. https://doi.org/10.1002/aic.15802.
- Liu P, LaMarche CQ, Kellogg KM, Leadley S, Hrenya CM. Cohesive grains: bridging microlevel measurements to macrolevel flow behavior via surface roughness. AIChE J. 2016;62:1-9. https://doi.org/10. 1002/aic.15383.
- LaMarche CQ, Liu P, Kellogg KM, Hrenya CM. Fluidized-bed measurements of carefully-characterized, mildly-cohesive (Group A) particles. Chem Eng J. 2017;310 Part 1:259-271. https://doi.org/10.1016/j.cej.2016.10.119.
- Royer JR, Evans DJ, Oyarte L. High-speed tracking of rupture and clustering in freely falling granular streams. *Nature*. 2009;459(7250): 1-4. https://doi.org/10.1038/nature08115.
- Rabinovich YI, Adler JJ, Ata A, Singh RK, Moudgil BM. Adhesion between nanoscale rough surfaces. J Colloid Interface Sci. 2000;232 (1):10-16. https://doi.org/10.1006/jcis.2000.7167.
- Chaudhuri B, Muzzio FJ, Tomassone MS. Modeling of heat transfer in granular flow in rotating vessels. *Chem Eng Sci.* 2006;61(19):6348-6360. https://doi.org/10.1016/j.ces.2006.05.034.
- Molerus O. Heat transfer in moving beds with a stagnant interstitial gas. Int J Heat Mass Transf. 1997;40(17):4151-4159. https://doi.org/ 10.1016/s0017-9310(97)00030-6.
- Buonanno G, Carotenuto A. The effective thermal conductivity of a porous medium with interconnected particles. *Int J Heat Mass Transf.* 1997;40(2):393-405. https://doi.org/10.1016/0017-9310 (96)00111-1.
- Rong D, Horio M. DEM simulation of char combustion in a fluidized bed. Second International Conference on CFD in Minerals and Process Industries CSIRO; December 6–8; Melbourne, Australia, 1999:65-70.
- Vargas WL, McCarthy JJ. Conductivity of granular media with stagnant interstitial fluids via thermal particle dynamics simulation. *Int J Heat Mass Transf.* 2002;45(24):4847-4856. https://doi.org/10.1016/s0017-9310(02)00175-8.
- Delvosalle C, Vanderschuren J. Gas-to-particle and particle-to-particle heat transfer in fluidized beds of large particles. *Chem Eng Sci.* 1985;40(5):769-779. https://doi.org/10.1016/0009-2509(85) 85030-2.
- Ofuchi K, Kunii D. Heat-transfer characteristics of packed beds with stagnant fluids. Int J Heat Mass Transf. 1965;8(5):749-757. https://doi.org/10.1016/0017-9310(65)90021-9.
- Yagi S, Wakao N. Heat and mass transfer from wall to fluid in packed beds. AIChE J. 1959;5(1):79-85. https://doi.org/10.1002/aic. 690050118.
- Denloye A, Botterill J. Heat transfer in flowing packed beds. Chem Eng Sci. 1977;32(5):461-465. https://doi.org/10.1016/0009-2509 (77)87001-2.
- Patton JS, Sabersky RH, Brennen CE. Convective heat transfer to rapidly flowing, granular materials. *Int J Heat Mass Transf.* 1986;29(8): 1263-1269. https://doi.org/10.1016/0017-9310(86)90159-6.
- Sullivan WN, Sabersky RH. Heat transfer to flowing granular media. Int J Heat Mass Transf. 1975;18(1):97-107. https://doi.org/10.1016/0017-9310(75)90012-5.
- Spelt JK, Brennen CE, Sabersky RH. Heat transfer to flowing granular material. Int J Heat Mass Transf. 1982;25(6):791-796. https://doi.org/ 10.1016/0017-9310(82)90091-6.
- Gloski D, Glicksman L, Decker N. Thermal resistance at a surface in contact with fluidized bed particles. *Int J Heat Mass Transf.* 1984;27 (4):599-610. https://doi.org/10.1016/0017-9310(84)90032-2.
- Chaudhuri B, Muzzio FJ, Tomassone MS. Experimentally validated computations of heat transfer in granular materials in rotary calciners. *Powder Technol*. 2010;198(1):6-15. https://doi.org/10.1016/j.powtec. 2009.09.024.
- Komossa H, Wirtz S, Scherer V, Herz F, Specht E. Heat transfer in indirect heated rotary drums filled with monodisperse spheres:

- comparison of experiments with DEM simulations. *Powder Technol.* 2015;286:722-731. https://doi.org/10.1016/j.powtec.2015.07.022.
- Herz F, Mitov I, Specht E, Stanev R. Influence of the motion behavior on the contact heat transfer between the covered wall and solid bed in rotary kilns. Exp Heat Transf. 2014;28(2):174-188. https://doi.org/ 10.1080/08916152.2013.854283.
- Nafsun Al, Herz F, Specht E, Scherer V, Wirtz S. Heat transfer experiments in a rotary drum for a variety of granular materials. *Exp Heat Transf.* 2016;29(4):520-535. https://doi.org/10.1080/08916152. 2015.1036180.
- Thammavong P, Debacq M, Vitu S, Dupoizat M. Experimental apparatus for studying heat transfer in externally heated rotary kilns. *Chem Eng Technol.* 2011;34(5):707-717. https://doi.org/10.1002/ceat.201000391.
- Golob M, Jeter S, Sadowski D. Heat transfer coefficient between flat surface and sand. ASME 2011 5th International Conference on Energy Sustainability; August 7–10; Washington DC, 2011:1441-1450. https://doi.org/10.1115/ES2011-54438.
- Rabinovich YI, Adler JJ, Ata A, Singh RK, Moudgil BM. Adhesion between nanoscale rough surfaces. *J Colloid Interface Sci.* 2000;232 (1):17-24. https://doi.org/10.1006/jcis.2000.7168.
- LaMarche CQ, Leadley S, Liu P, Kellogg KM, Hrenya CM. Method of quantifying surface roughness for accurate adhesive force predictions. Chem Eng Sci. 2017;158(C):140-153. https://doi.org/10.1016/j. ces.2016.09.024.
- Fuller KNG, Tabor D. The effect of surface roughness on the adhesion of elastic solids. Proc R Soc Lond A. 1975;345(1642):327-342. https://doi.org/10.1098/rspa.1975.0138.
- Cooper MG, Mikic BB, Yovanovich MM. Thermal contact conductance. J Heat Mass Transf. 1969;12(3):279-300. https://doi.org/10.1016/0017-9310(69)90011-8.
- Mikic BB. Thermal contact conductance; theoretical considerations. *Int J Heat Mass Transf.* 1974;17(2):205-214. https://doi.org/10.1016/ 0017-9310(74)90082-9.
- 45. Wolff EG, Schneider DA. Prediction of thermal contact resistance between polished surfaces. *Int J Heat Mass Transf*. 1998;41(22):3469-3482. https://doi.org/10.1016/S0017-9310(98)00067-2.
- Batchelor GK, O'brien RW. Thermal or electrical conduction through a granular material. *Proc R Soc Lond A*. 1977;355(1682):313-333. https://doi.org/10.1098/rspa.1977.0100.
- LaMarche CQ, Miller AW, Liu P, Hrenya CM. Linking micro-scale predictions of capillary forces to macro-scale fluidization experiments in humid environments. AIChE J. 2016;62:3585-3597. https://doi.org/ 10.1002/aic.15281
- 48. Utermann S, Aurin P, Benderoth M, Fischer C, Schröter M. Tailoring the frictional properties of granular media. *Phys Rev E*. 2011;84(3): 031306. https://doi.org/10.1103/PhysRevE.84.031306.
- LaMarche CQ, Miller AW, Liu P, Leadley S, Hrenya CM. How nanoscale roughness impacts the flow of grains influenced by capillary cohesion. AIChE J. 2017;116(9):098001-095257. https://doi.org/10. 1002/aic.15830.
- Wang S, Hu Y-Z, Wang W-Z, Wang H. Effects of surface roughness on sliding friction in lubricated-point contacts: experimental and numerical studies. J Tribol. 2007;129(4):809-809. https://doi.org/10. 1115/1.2768081.
- Karupannasamy DK, de Rooij MB, Schipper DJ. Multi-scale friction modelling for rough contacts under sliding conditions. Wear. 2013; 308(1-2):222-231. https://doi.org/10.1016/j.wear.2013.09.012.
- 52. Brilliantov NV, Spahn F, Hertzsch J-M, Pöschel T. Model for collisions in granular gases. *Phys Rev E*. 1996;53(5):5382-5392. https://doi.org/10.1103/PhysRevE.53.5382.

- Stronge WJ. Rigid body collisions with friction. *Proc R Soc Lond A*. 1990;431(1881):169-181. https://doi.org/10.1098/rspa.1990.0125.
- 54. Schluender EU. Heat transfer to packed and stirred beds from the surface of immersed bodies. *Chem Eng Process.* 1984;18(1):31-53. https://doi.org/10.1016/0255-2701(84)85007-2.
- Kuipers JAM, Prins W, Van Swaaij WPM. Numerical calculation of wall-to-bed heat-transfer coefficients in gas-fluidized beds. AIChE J. 1992;38(7):1079-1091. https://doi.org/10.1002/aic.690380711.
- Johnson PC, Nott P, Jackson R. Frictional-collisional equations of motion for participate flows and their application to chutes. *J Fluid Mech.* 1990;210(1):501-535. https://doi.org/10.1017/s0022112090001380.
- Jerkins M, Schröter M, Swinney HL, Senden TJ, Saadatfar M, Aste T.
 Onset of mechanical stability in random packings of frictional spheres.
 Phys Rev Lett. 2008;101(1):018301. https://doi.org/10.1103/PhysRevLett.101.018301.
- 58. Tsotsas E, Martin H. Thermal conductivity of packed beds: a review. *Chem Eng Process.* 1987;22(1):19-37. https://doi.org/10.1016/0255-2701(87)80025-9.
- David Scott G. Packing of spheres: packing of equal spheres. *Nature*. 1960;188(4754):908-909. https://doi.org/10.1038/188908a0.
- Syamlal M, Rogers W, Brien TJO. MFIX Documentation Theory Guide; 1993. https://doi.org/10.2172/10145548.
- Lattanzi AM, Hrenya CM. A coupled, multiphase heat flux boundary condition for the discrete element method. *Chem Eng J.* 2016;304(C): 766-773. https://doi.org/10.1016/j.cej.2016.07.004.
- 62. Musserj. https://mfix.netl.doe.gov. April 2016:1-128.
- Al-Ansary H, El-Leathy A, Al-Suhaibani Z, et al. Experimental study of a sand-air heat exchanger for use with a high-temperature solar gas turbine system. J Sol Energy Eng. 2012;134(4):041017-041017. https://doi.org/10.1115/1.4007585.
- 64. Onoda GY, Liniger EG. Random loose packings of uniform spheres and the dilatancy onset. *Phys Rev Lett.* 1990;64(22):2727-2730. https://doi.org/10.1103/PhysRevLett.64.2727.
- Suzuki M, Shinmura T, Iimura K, Hirota M. Study of the wall effect on particle packing structure using X-ray micro computed tomography. Adv Powder Technol. 2008;19(2):183-195. https://doi.org/10.1163/ 156855208X293817.
- 66. Math-Works IMT, Inc. 1995. Partial Differential Equation Toolbox User"S Guide."
- Hyde M, Klocke HJ. Heat transfer between fluidized beds and heat exchange installations. *Int Chem Eng.* 1980;20(4):583-599.
- Quintanilla MAS, Castellanos A, Valverde JM. Correlation between bulk stresses and interparticle contact forces in fine powders. *Phys Rev* E. 2001;64(3):031301. https://doi.org/10.1103/PhysRevE.64.031301.
- Oschmann T, Schiemann M, Kruggel-Emden H. Development and verification of a resolved 3D inner particle heat transfer model for the discrete element method (DEM). *Powder Technol.* 2016;291(C): 392-407. https://doi.org/10.1016/j.powtec.2015.12.008.

How to cite this article: Mishra I, Lattanzi AM, LaMarche CQ, Morris AB, Hrenya CM. Experimental validation of indirect conduction theory and effect of particle roughness on wall-to-particle heat transfer. *AIChE J.* 2019;65:e16703. https://doi.org/10.1002/aic.16703